PAPER

Check for updates

Electrospun superhydrophilic membranes for effective removal of Pb(II) from water†

Linlin Zang,[a] Ru Lin,[a] Tianwei Dou,[b] Lu wang,[a] Jun Ma (ID) *[a] and Liguo Sun (ID) *[b]

Nanofibrous membranes have a high specific surface area and large porosity, which are beneficial for being used as adsorbents to remove heavy metal ions from water. In this work, electrospun nanofibers were wrapped with a hydrogel layer with a tunable thickness, which endowed the membrane with excellent superhydrophilic performance. Because of good water-retention properties and abundant functional groups originating from the hydrogel layer, as a static adsorbent, the maximum adsorption capacity of Pb(II) was up to 146.21 mg g^{-1} according to the Langmuir model. Meanwhile, the electrospun membrane also possessed water permeability as a flow-through membrane for dynamic adsorption, which was obviously different from traditional hydrogel adsorbents. As a result, the rejection ratio of Pb(II) can remain over 55% after running for 72 h under high pH conditions and at low initial ion concentrations. Apart from these, cycle operations confirmed the regeneration of the membrane, and competitive adsorption experiments illustrated the selective removal of Pb(II) in a mixed ion solution.

Introduction

In recent years, fast industrialization and blooming growth have been substantially contributing to environmental pollution. Notably, heavy metal ions are considered as the major inorganic contaminants because of their mobility in the aqueous ecosystem, extreme toxicity and non-biodegradable nature.[1-4] Moreover, due to their bioaccumulation in biological tissues *via* the food chain, heavy metal ions are also harmful to our health. For example, the lead ion (Pb(II)) can damage the nervous system, digestive system, immunological system, kidneys and so on.[5-7] At present, various physical and chemical methods (electro-dialysis, chemical precipitation, *etc.*) have been used to solve this problem. However, these conventional technologies have several drawbacks, such as large investment, high energy consumption, complex post-treatment and secondary pollution.[8,9] Therefore, some efficient methods and materials are needed to remove Pb(II) from the aquatic ecosystem.

Electrospinning is a simple and promising technique for generating nanofibrous membranes with fiber diameters in the range of nanometers to a few microns, and matrix materials of the membranes come from a variety of polymers.[10-12] Because of their controllable thicknesses, high porosity and large surface area, electrospun nanofibrous membranes (ENMs) have many applications in the environment, catalysis, energy, medicine and so on.[13-22] Due to its large pore size and high flux, the ENM is often used as a pretreatment which mainly involves a sieving mechanism. However, through modifying the functional polymer or doping nanoparticles,[23-29] it can also achieve the adsorptive separation of bivalent or multivalent ions whose sizes are much smaller than the pore sizes of the membrane. Therefore, the ENM has gradually become an ideal adsorptive material for removing toxic metal ions in aqueous solution. For example, due to its high specific surface area and abundant adsorption active sites, the maximum adsorption capacity of a thiol-modified cellulose nanofibrous composite membrane for Pb(II) was found to be 137.7 mg g^{-1} which was higher than those of organic/inorganic nanocomposites such as 64.5 mg g^{-1} for Fe$_3$O$_4$/cyclodextrin polymer nanocomposites and 91.8 mg g^{-1} for magnetic attapulgite/fly ash/poly(acrylic acid) nanocomposites.[30-32] However, the ENM had slower adsorption kinetics and lower adsorption capacities, compared with hydrogel adsorbents which possessed a three-dimensional polymer network, abundant hydrophilic functional groups and good water retention properties.[33-35] For instance, poly(acrylic acid) (PAA) is a kind of abundant carboxyl-containing polymer frequently reported. Many researchers utilized it to fabricate monolithic hydrogels or microgels to adsorb heavy metal ions as the static adsorbents.[36-41] Recently, combining the properties of hydrogels with the structure of the ENM, electrospun hydrogel membranes (EHMs) have started to draw great attention in biomedicine and engineering.[42-45] However, few studies are reported about the use of EHMs as static adsorbents and flow-through membranes in dynamic processes.

[a]State Key Laboratory of Urban Water Resource and Environment, School of Environment, Harbin Institute of Technology, Harbin 150090, PR China. E-mail: majunhit@126.com

[b]Key Laboratory of Chemical Engineering Process & Technology for High-efficiency Conversion, College of Heilongjiang Province, School of Chemical Engineering and Materials, Heilongjiang University, Harbin, 150080, PR China. E-mail: sunliguo1975@163.com

† Electronic supplementary information (ESI) available. See DOI: 10.1039/c8na00044a

Herein, according to all of the above, we presented a novel adsorptive membrane made up of cellulose acetate and poly-(methacrylic acid) *via* the electrospinning technique. Our work aimed at the following four aspects: (1) presenting a facile electrospinning method to fabricate hydrogel-wrapped nanofibers, which can be utilized to selectively adsorb Pb(ii) from aqueous solutions; (2) overcoming the poor functional modification and limited adsorption capacity of the conventional membranes to some extent;[46–48] (3) providing a kind of environment-friendly adsorbent to avoid damage to the ecological system caused by the entrance of doped inorganic nanomaterials into water; and (4) breaking through the limitation of traditional hydrogels only as static adsorbents. This paper provided a new perspective in the fabrication of nanofibers wrapped by a hydrogel polymer and the application of the EHM as a flow-through membrane in dynamic adsorption processes. Therefore, this study demonstrated that the cellulose acetate/poly(methacrylic acid) nanofibrous membrane (CPNM) might be highly promising in the removal of Pb(ii) from aqueous solutions.

Experimental

Materials

Cellulose acetate, copper chloride, cadmium nitrate, nickel nitrate, lead nitrate, sodium hydroxide and EDTA were provided by Sinopharm Chemical Reagent Co., Ltd. *N,N*-Dimethylformamide (DMF) was purchased from Tianjin Kemiou Chemical Reagent Co., Ltd. Methacrylic acid (MAA) was purchased from Aladdin Reagent Co. and treated before being used. All chemical reagents were of analytical grade.

Methods

Typically, the mass ratios of CA and PMAA were 1 : 1, 2 : 1 and 3 : 1, which were added into DMF and fully stirred. The method of synthesising poly(methacrylic acid) PMAA is provided in the ESI.† The total mass factions of CA and PMAA in spinning solutions were all fixed at 15 wt%. The pushing rate was fixed at 2 mL h^{-1} using a micro-injection pump (LSP01-1A, Longer Pump, Halma Inc.). The working voltage was 17 kV and the nanofibers were collected by a rotary roller. The receiving distance was fixed at 30 cm. The spinning temperature and humidity were fixed at 20.8 ± 2 °C and 30.5 ± 2%, respectively. The obtained EHMs were placed in an oven at 50 °C for one night, and then were pressed at 90 °C. The as-prepared EHMs were heat-treated at 150 °C for 1 h in an oven, and different weight ratios of CA and PMAA (1 : 1, 2 : 1 and 3 : 1) were labelled as CPNM-1, CPNM-2 and CPNM-3, respectively.

Characterization

The surface morphology of the membrane was characterized by field emission scanning electron microscopy (Hitachi S4800, Japan). A field emission transmission electron microscope (JEM-2100, Japan) was used to observe the inner structure of a single nanofiber. The functional groups and elements of the membrane were detected by FT-IR spectra (Spectrum one, USA)

and X-ray photo-electron spectroscopy (XPS, ESCALAB 250Xi, USA). The Pb(ii) concentrations were detected using an inductively coupled plasma-optical emission spectrometer (ICP-OES, Optima 8300, PerkinElmer, USA). The tensile strength of the membrane was determined using a CMT4000 testing machine (China). The membranes were cut into 50 mm × 10 mm rectangle samples before testing, and the stretching rate was fixed at 10 mm min^{-1}. The membrane porosity was determined by the fluid displacement method.[49]

The effects of environmental conditions on the adsorption capacity were investigated in a 50 mL centrifuge tube. The effect of solution pH was investigated at pH 2–6. The adsorbent doses were 1 g L^{-1} and the initial concentration of Pb(ii) was 60 mg L^{-1}. The effect of PMAA content was examined with CPNMs (1 : 1, 2 : 1 and 3 : 1), and other conditions were the same as those of pH investigation. The initial Pb(ii) concentrations (C_0) were 10 to 100 mg L^{-1} (adsorption isothermal experiments). The effect of contact time was observed in the Pb(ii) solution (60 mg L^{-1}, pH = 6) for 1–180 min (kinetic assays).

To study uptake selectivity, the competitive adsorption was investigated in multi-component mixtures (Ni(ii), Cu(ii), Cd(ii) and Pb(ii)). The ion concentration of each ion was 25 mg L^{-1} and the pH was 6. In terms of reusability experiments, 30 mL Pb(ii) solution (100 mg L^{-1}) was adsorbed by 30 mg adsorbents and shaken for 3 h at 25 °C. For the desorption test, the adsorbents were shaken in 30 mL of 0.1 M EDTA solution for 10 h.

The dynamic adsorption experiments were performed in a dead-end filtration device and the separation process was driven by gravity. Pb(ii) solutions with different concentrations were prepared using Millipore water. The feed was supplied continuously to the cell. The membranes were placed in the cell and compacted at 0.05 MPa to obtain a steady flux before testing.

Results and discussion

Characterization of the CPNMs

The SEM images of the membranes are shown in Fig. 1a–c. The surface morphology of the nanofibers was all smooth after thermal treatment. Through Image J software, the average
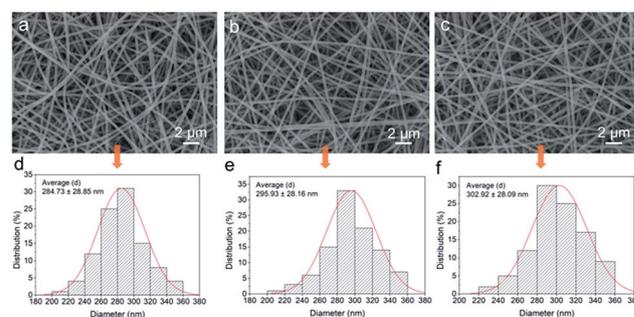

Fig. 1 SEM images of the nanofibers with different mass ratios of CA and PMAA: (a) CPNM-1, (b) CPNM-2, and (c) CPNM-3; (d), (e) and (f) are their corresponding diameter distribution.

diameters of the nanofibers can be calculated. Fig. 1d–f show that the average values had a slight decline from 302.92 ± 28.09 nm to 284.73 ± 28.85 nm with the mass ratios of PMAA to CA increasing. The TEM images clearly present the core–shell structure of the nanofiber (Fig. 2). Due to the difference of molecular chain activity between the two kinds of polymers, the structure formed in a solvent evaporation process. The relatively dark part of the TEM image was CA and the light area was the PMAA shell. The average thickness of the PMAA shell and diameter of the CA core are listed in Table S1.† The above results indicated that core–shell nanofibers with adjustable thicknesses of the hydrogel layer could be fabricated *via* a simple, fast, economical and environmentally friendly method, which was significantly different from many traditional modification methods.

Taking CPNM-1 as an example, the membrane consisting of thousands of core–shell nanofibers was white and flexible (Fig. 3a). When a water droplet came into contact with the surface of the membrane, the water contact angle was 0° in air (Fig. 3b), which was quite beneficial for adsorbents in an aqueous system. After the membrane was completely immersed in water with different pH values (2–6), it reached a hydrogel membrane state (Fig. 3c). The above phenomena revealed the superhydrophilic properties of the CPNM, which further identified that the nanofiber was composed of a hydrophilic PMAA shell and a hydrophobic CA core. Moreover, Table S1† shows several physical parameters about the CPNMs. The data showed that the porosity of the CPNM was above 75%, and the tensile strength had an increasing trend as the content of CA decreased.

Fig. 4a shows the FTIR spectra of the CPNMs with different mass ratios of CA and PMAA. They had the same characteristic absorption peaks, for example, the C=O stretching vibration peaking around 1740 cm^{-1} where the strong peak belonged to PMAA. There existed a broad band at 3000–3660 cm^{-1} assigned to the O–H stretching vibration.[50] The carboxyl groups had a weak peak at 1368 cm^{-1} which was assigned to –COO– symmetric stretching vibrations.[51] Cellulose had two obvious peaks at 1040 and 1229 cm^{-1}, which were assigned to C–O and C–O–C bond vibrations, respectively.[52,53] The XPS test was performed to further investigate the elemental composition of the CPNM. Fig. 4b shows the wide-scan spectrum of the CPNM and the peaks of C1s and O1s can be obviously observed. Fig. 4c shows that the C1s is divided into three peaks. The binding energy of 284.8 eV was attributed to C–C. The peaks at 286.5 and 288.9 eV could be assigned to C–O and C=O, respectively. As for the O1s spectrum, as shown in Fig. 4d, the fitted peak at the

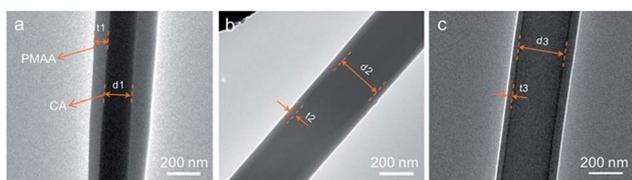binding energy of 531.2 and 532.3 eV belonged to C=O and C–O, respectively.

Adsorption kinetics

The adsorption rate is one of the key aspects affecting the adsorption performance. Three kinetic models, namely the pseudo-first-order model and pseudo-second-order model and intra-particle-diffusion model, were established to describe the controlling mechanism of the Pb(II) adsorption process, such as mass transfer and chemical reaction. Therefore, we investigated the kinetic curves of Pb(II) adsorption, and the parameters of the three kinetic models are presented in Fig. 5 and Table S2.† For the CPNMs, according to the pseudo-first-order kinetic model, their $q_{e,cal}$ values were 16.92, 14.71 and 10.33 mg g^{-1}, respectively, which were not consistent with the experimentally observed $q_{e,exp}$ values (37.6, 43.4 and 53.8 mg g^{-1}). And R^2 values of the pseudo-second-order kinetic model were all below 0.9997. Therefore, the results indicated that Pb(II) adsorption followed
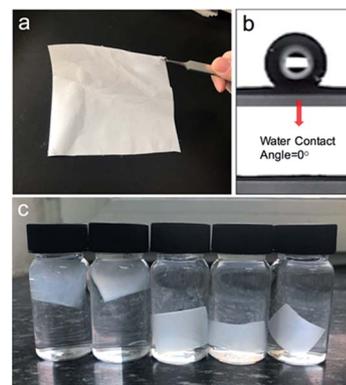

Fig. 3 (a) Photograph of the white and flexible CPNM; (b) photograph of the water contact angle in air; (c) the digital photo of the CPNM in DI water with different pH values (2–6, from right to left).

Fig. 2 (a), (b) and (c) are the corresponding TEM images of CPNM-1, CPNM-2 and CPNM-3, respectively.
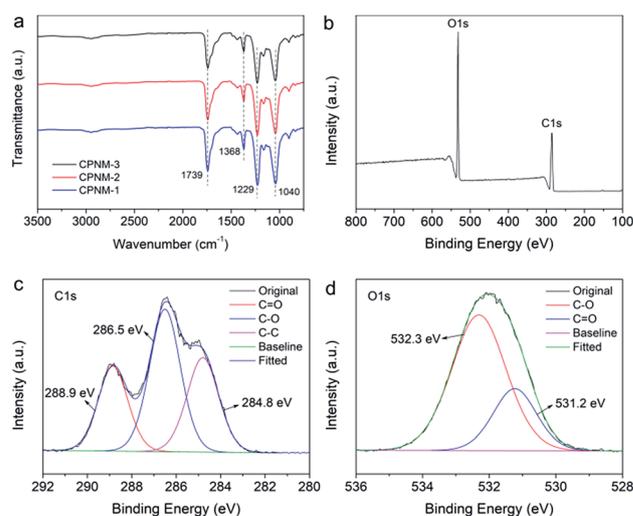

Fig. 4 (a) FTIR spectra of the CPNMs; (b) XPS wide-scan spectrum of the CPNM; (c) and (d) are C1s and O1s spectra, respectively.
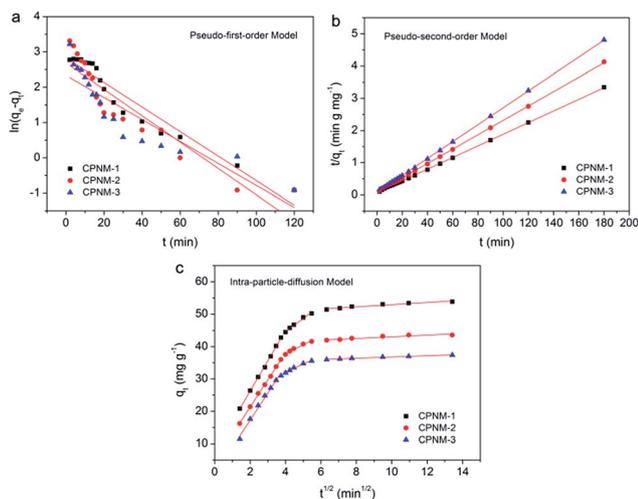
Fig. 5 (a) The pseudo-first-order kinetic model, (b) the pseudo-second-order kinetic model, (c) and the intra-particle-diffusion kinetics for the adsorption of Pb(II) by the CPNMs.

the pseudo-second-order kinetic model which involved chemical interactions, such as electron exchange or sharing between Pb(II) and binding sites of the membrane.

As shown in Fig. 5c, the intra-particle-diffusion curves were non-linear, indicating the complex adsorption process of Pb(II) by the CPNMs. The whole diffusion process was decided by three steps. The first step represented the diffusion process of Pb(II) from the solution to the external surface of the membranes. The second step presented further intra-particle diffusion from the surface to the inside part of the membranes. The third step occurred at the equilibrium adsorption stage. The parameters k_1, k_2 and k_3 were the intra-particle diffusion rate constants of the three adsorption steps. The k_1 values were higher than k_2 and k_3 values, indicating the fast transfer and adsorption of Pb(II) from the solution to the surface of the membranes. As the adsorption time increased, the binding sites reduced and were occupied by Pb(II), leading to the slow intra-particle diffusion rate in the second and third step.

Adsorption isotherms

Adsorption isotherm studies are remarkably significant to determine the efficiency and capacity of adsorption. The Langmuir and Freundlich models are commonly used to describe adsorption isotherms. The Langmuir isotherm equation is suitable for the ideal monolayer adsorption and no interactions between the adsorbed molecules, and the Freundlich isotherm model is more often used to describe chemisorption properties.[44]

The fitting lines and corresponding parameters of the two models are shown in Fig. 6 and Table 1. It can be seen that the R^2 value was higher (>0.99) when the adsorption mechanism was described by the Langmuir isotherm. The result indicated that Pb(II) adsorption occurred in a monolayer manner on the homogeneous surface of the CPNMs. And the maximum adsorption capacity (Q_{max}) rose from 49.75 to 146.21 mg g^{-1} with PMAA content increasing. Therefore, the Pb(II) adsorption
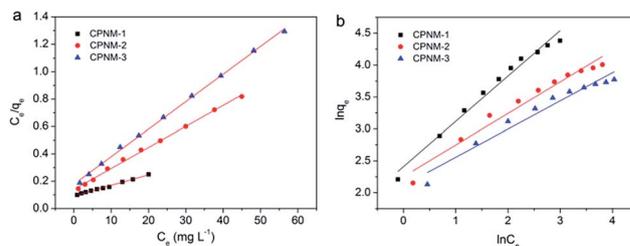

Fig. 6 (a) Langmuir and (b) Freundlich models for the adsorption of Pb(II) by the CPNMs.

Table 1 Langmuir and Freundlich models for the adsorption of Pb(II) by the CPNMs

Samples	Langmuir			Freundlich		
	R^2	Q_{max}	K_L	R^2	$1/n$	K_F
CPNM-1	0.9935	146.21	0.0828	0.9808	0.7102	11.1275
CPNM-2	0.9974	68.14	0.1102	0.9635	0.4948	9.5151
CPNM-3	0.9987	49.75	0.1128	0.9549	0.4424	8.2744

capacity can be controlled via changing the thickness of the hydrogel layer to a certain degree.

Selectivity performance and reusability study

In a mixed solution of bivalent metal ions, their q_e values followed the sequence Pb(II) > Cu(II) > Cd(II) > Ni(II), and Pb(II) had the highest q_e value (Fig. 7a). This order was consistent with the first stability constants of the associated metal acetate: log K_1 = 2.52, 2.16, 1.5, and 1.2 for Pb(COO)$^+$, Cu(COO)$^+$, Cd(COO)$^+$, and Ni(COO)$^+$, respectively.[44] As shown in Table S3,† the K_D sequence (Pb(II) > Cu(II) > Cd(II) > Ni(II)+) and α (Pb(II)/M^{n+}) indicated that the CPNM favored the capture of Pb(II).

The desorption characteristics of CPNM-1 in 0.1 M EDTA solution are presented in Fig. 7b. After 1 cycle, due to the sufficient occupation of adsorption sites on CPNM-1, Pb(II) adsorption can eventually reach saturation. However, it can be seen that the q_e values of Pb(II) decreased obviously from 80 to 58 mg g^{-1} after 5 cycles. The result was because some of the Pb(II) ions which were not desorbed by EDTA occupied the
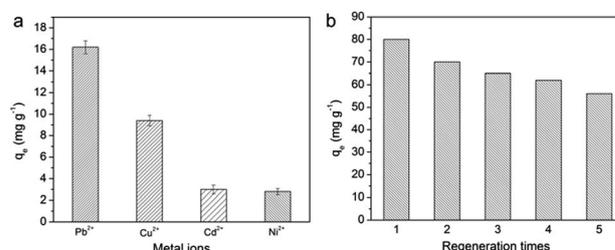

Fig. 7 (a) Pb(II) competitive uptake in a mixed bivalent metal ion solution (pH = 6; V = 30 mL; m [adsorbent] = 30 mg; C_0 [Pb(II)] = 25 mg L^{-1}; 25 °C); (b) regeneration times of the adsorption process for Pb(II) removal by CPNM-1 (pH = 6; V = 30 mL; m [adsorbent] = 30 mg; C_0 [Pb(II)] = 100 mg L^{-1}; 25 °C).

adsorption sites. Besides, the SEM images (Fig. S2†) indicated that the surface of the nanofibers became rough after adsorption and desorption, which was quite different from the smooth surface of the initial nanofibers. The reason was that the ion-exchange process led to the shrinkage of PMAA molecules and deformation of the nanofibers.

Dynamic adsorption experiments

The suitability of the CPNM as a flow-through membrane adsorber was further investigated. Fig. 8a shows the curves of rejection ratios under different pH environments. It can be seen that the pH value significantly affects the rejection ratio of Pb(II) in the dynamic adsorption process. As the pH value decreased, the adsorption equilibrium time of Pb(II) became obviously shorter and the rejection rates of Pb(II) witnessed a more dramatic decline in the initial stage of the adsorption process. The reasons were that low pH values led to fewer adsorption sites, depressing the Pb(II) exchange reaction, and shortening the contact time between the membrane and Pb(II). However, under high pH value conditions, the functional groups of PMAA were deprotonated resulting in more binding sites, and higher adsorption capacity and rejection rates. When the pH value was 6, the rejection rate of Pb(II) still remained above 55% after operating for 72 h, while the rejection rates decreased to 0% at pH values <6. Therefore, the result suggested that relatively high pH values were conducive to the removal of Pb(II) in the dynamic adsorption process.

Fig. 8b shows the effect of different initial concentrations of Pb(II) on the rejection rate. As the initial concentration increased, more Pb(II) took part in ion-exchange with the membrane. As a result, the swelling degree of the PMAA shell dramatically decreased, and then the contact time between the

solution and the membrane also decreased accordingly. When the initial concentration of Pb(II) in aqueous solution increased from 10 mg L^{-1} to 50 mg L^{-1}, the adsorption equilibrium time shortened from 72 h to 27 h. The results indicated that the low initial Pb(II) concentration was beneficial to the dynamic adsorption of the CPNM.

In addition, CPNM-2 and CPNM-3 were also operated as the flow-through membranes. As shown in Fig. 8c, the adsorption equilibrium time of the CPNM-2 and the CPNM-3 was below 13 h, which was shorter than that of CPNM-1 under the same conditions. According to the above results, high pH values of solution, low initial ion concentration and a thick hydrogel layer in nanofibers can effectively improve the rejection rate of Pb(II) during the dynamic adsorption process.

Conclusions

This work presented a kind of adsorptive membrane made of hydrogel polymer wrapped nanofibers *via* a uniaxial electrospinning process. The functional shell of the nanofibers provided abundant available adsorption sites between the surface and interior of the nanofibers. The adsorption capacity was affected by pH, initial ion concentration, contact time and the contents of the functional polymer. Under the optimized conditions, the rejection rates of Pb(II) by the CPNM were up to 95%. The CPNM could be reused after desorption and had selective adsorption for Pb(II) in a mixed divalent ion solution. In addition, the CPNM can be used as the dynamic adsorption membrane, and the rejection ratio of Pb(II) can remain above 55% after running for 72 h when the initial concentration was 10 mg L^{-1} under pH 6 conditions. The above results demonstrated that the CPNM has great potential as the adsorptive membrane for Pb(II) removal.

Conflicts of interest

There are no conflicts to declare.

Acknowledgements

Fig. 8 Continuous filtration operation: (a) rejection rates of the CPNM-1 to Pb(II) aqueous solution under different pH environments (pH = 2–6; C_0 = 10 mg L^{-1}; 25 °C); (b) rejection rates of the CPNM-1 to Pb(II) aqueous solution with different initial concentrations (pH = 5; C_0 = 10–50 mg L^{-1}; 25 °C); (c) changes of rejection ratio of the CPNM-2 and CPNM-3 to Pb(II) aqueous solution with filtration time (pH = 5; C_0 = 10 mg L^{-1}; 25 °C).

Notes and references

1 W. Liu, N. Xu, T. Wang, L. Xiong and J. Ni, *Chem. Eng. J.*, 2013, **215**, 366–374.
2 Y. Pang, G. Zeng, L. Tang, Y. Zhang, Y. Liu, X. Lei, Z. Li, J. Zhang and G. Xie, *Desalination*, 2011, **281**, 278–284.
3 T. A. Saleh, *Desalin. Water Treat.*, 2015, **57**, 1–15.
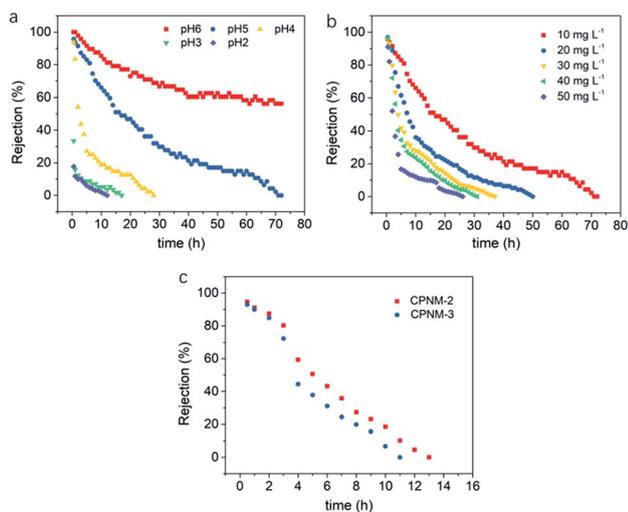4 Y. Liu, L. Wang, X. C. Wang, Z. S. Huang, C. B. Xu and J. Ma, *Water Res.*, 2017, **124**, 149–157.

5 Y. X. Liu, J. M. Yan, D. X. Yuan, Q. L. Li and X. Y. Wu, *Chem. Eng. J.*, 2013, **218**, 81–88.

6 K. Nemsadze, T. Sanikidze, L. Ratiani, L. Gabunia and T. Sharashenidze, *Georgian Med. News*, 2009, **172–173**, 92–96.

7 C. H. Yan, J. Xu and X. M. Shen, *Environ. Health Perspect.*, 2013, **121**, A294–A295.

8 P. K. Holt, G. W. Barton and C. A. Mitchell, *Chemosphere*, 2005, **59**, 355–367.

9 H. Tokuyama, T. Yoshida and L. L. He, *Ind. Eng. Chem. Res.*, 2011, **50**, 10270–10277.

10 Z. Liu, D. D. Sun, P. Guo and J. O. Leckie, *Nano Lett.*, 2007, **7**, 1081–1085.

11 X. Lu, J. Zhou, Y. Zhao, Y. Qiu and J. Li, *Chem. Mater.*, 2008, **20**, 3420–3424.

12 Q. Bao, H. Zhang, J. X. Yang, S. Wang, D. Y. Tang, R. Jose, S. Ramakrishna, C. T. Lim and K. P. Loh, *Adv. Funct. Mater.*, 2010, **20**, 782–791.

13 J. G. Lee, E. J. Lee, S. Jeong, J. Guo, A. K. An and H. Guo, *J. Membr. Sci.*, 2017, **526**, 395–408.

14 M. Obaid, G. M. K Tolba, M. Motlak, O. A. Fadali, K. A. Khalil and A. A. Almajid, *Chem. Eng. J.*, 2015, **279**, 631–638.

15 X. Zhao, W. Shan, Y. Xia, J. Yu and B. Ding, *Sci. Rep.*, 2016, **6**, 35472.

16 S. W. Choi, J. Y. Park and S. K. Sang, *Chem. Eng. J.*, 2011, **172**, 550–556.

17 Y. Si, X. Wang, C. Yan, L. Yang, J. Yu and B. Ding, *Adv. Mater.*, 2016, **28**, 9655.

18 X. Wang, L. Dou, L. Yang, J. Yu and B. Ding, *J. Hazard. Mater.*, 2016, **324**, 203–212.

19 S. J. Doh, C. Kim, S. G. Lee, S. J. Lee and H. Kim, *J. Hazard. Mater.*, 2008, **154**, 118–127.

20 Y. E. Miao, G. N. Zhu, H. Hou, Y. Y. Xia and T. Liu, *J. Power Sources*, 2013, **226**, 82–86.

21 C. Kim, K. Yang, M. Kojima, K. Yoshida and Y. Kim, *Adv. Funct. Mater.*, 2006, **16**, 2393–2397.

22 T. J. Sill and H. A. von Recum, *Biomaterials*, 2008, **29**, 1989–2006.

23 S. Xin, Z. Zeng, X. Zhou, W. Luo, X. Shi and Q. Wang, *J. Hazard. Mater.*, 2016, **324**, 365–372.

24 Y. Tian, M. Wu, R. Liu, Y. Li, D. Wang and J. Tan, *Carbohydr. Polym.*, 2011, **83**, 743–748.

25 N. Chitpong and S. M. Husson, *J. Membr. Sci.*, 2017, **523**, 418–429.

26 R. Zhao, X. Li, B. Sun, H. Ji and C. Wang, *J. Colloid Interface Sci.*, 2017, **487**, 297–309.

27 P. Tan, J. Wen, Y. Hu and X. Tan, *RSC Adv.*, 2016, **6**, 79641–79650.

28 M. Wang, X. Li, W. Hua, L. Shen, X. Yu and X. Wang, *ACS Appl. Mater. Interfaces*, 2016, **8**, 23995–24007.

29 U. Habiba, A. M. Afifi, A. Salleh and B. C. Ang, *J. Hazard. Mater.*, 2017, **322**, 182–194.

30 R. Yang, K. B. Aubrecht and H. Ma, *Polymer*, 2014, **55**, 1167–1176.

31 A. Z. M. Badruddoza, Z. B. Z. Shawon, W. J. D. Tay, K. Hidajat and M. S. Uddin, *Carbohydr. Polym.*, 2013, **91**, 322–332.

32 L. Jiang and P. Liu, *ACS Sustainable Chem. Eng.*, 2014, **2**, 1785–1794.

33 Y. K. Du, U. P. Shinde, B. Yeon and B. Jeong, *Prog. Polym. Sci.*, 2013, **38**, 672–701.

34 G. Bayramoğlu and A. M. Yakup, *Bioresour. Technol.*, 2009, **100**, 186–193.

35 Y. Liu, W. B. Wang and A. Q. Wang, *Desalination*, 2010, **259**, 258–264.

36 P. Liu, L. Jiang, L. Zhu and A. Wang, *React. Funct. Polym.*, 2014, **74**, 72–80.

37 A. T. Paulino, L. A. Belfiore, L. T. Kubota, E. C. Muniz, V. C. Almeida and E. B. Tambourgi, *Desalination*, 2011, **275**, 187–196.

38 C. Lin, C. Liu, G. Zhou, X. Rui, Y. Tang and Z. Zeng, *J. Hazard. Mater.*, 2015, **300**, 153–160.

39 G. Zhou, C. Liu, L. Chu, Y. Tang and S. Luo, *Bioresour. Technol.*, 2016, **219**, 451–457.

40 R. M. Yu, Y. Z. Shi, D. Z. Yang, Y. X. Liu, J. Qu and Z. Z. Yu, *ACS Appl. Mater. Interfaces*, 2017, **9**, 21809–21819.

41 Q. Fang and B. Chen, *J. Mater. Chem. A*, 2014, **2**, 8941–8951.

42 F. Xu, H. Sheardown and T. Hoare, *Chem. Commun.*, 2015, **52**, 1451–1454.

43 S. Lee, S. Yun, K. I. Park and J. H. Jang, *ACS Nano*, 2016, **10**, 3282–3294.

44 D. S. Puperi, A. Kishan, Z. E. Punske, Y. Wu, E. Cosgriffhernandez and J. L. West, *ACS Biomater. Sci. Eng.*, 2016, **4**, 1546–1558.

45 H. Qi, J. Cao, Y. Xin, X. Mao, D. Xie and J. Luo, *Mater. Sci. Eng., C*, 2017, **70**, 347–356.

46 S. An, M. Liou, K. Y. Song, H. S. Jo, M. W. Lee and S. S. Aldeyab, *Nanoscale*, 2015, **7**, 17778–17785.

47 T. H. Hwang, Y. M. Lee, B. S. Kong, J. S. Seo and J. W. Choi, *Nano Lett.*, 2012, **12**, 802–807.

48 C. Wang, K. W. Yan, Y. D. Lin and P. C. H. Hsieh, *Macromolecules*, 2010, **43**, 6389–6397.

49 A. L. Ahmad, N. Ideris, B. S. Ooi, S. C. Low and A. Ismail, *Desalination*, 2011, **278**, 318–324.

50 N. A. Kumar, H. J. Choi, Y. R. Shin, D. W. Chang, L. M. Dai and J. B. Baek, *ACS Nano*, 2012, **6**, 1715–1723.

51 M. J. Park, G. M. Nisola, E. L. Vivas, L. A. Limjuco, C. P. Lawagon and J. G. Seo, *J. Membr. Sci.*, 2016, **510**, 141–154.

52 P. M. Spasojevic, V. V. Panic, M. D. Jovic, J. Markovic, C. van Roost, I. G. Popovic and S. J. Velickovic, *J. Mater. Chem. A*, 2016, **4**, 1680–1693.

53 G. L. Huang, H. Y. Zhang, X. S. Jeffrey and T. G. Langrish, *Ind. Eng. Chem. Res.*, 2009, **48**, 2646–2651.

54 Y. He, X. Chen, S. Y. Bi, C. C. Shi, L. Chen and L. Y. Li, *Polym. Adv. Technol.*, 2013, **24**, 934–944.

55 J. Wang, P. Jia, K. Pan and B. Cao, *Desalin. Water Treat.*, 2015, **54**, 2856–2867.

56 Y. S. Ho and G. McKay, *Water Res.*, 1999, **33**, 578–584.

57 T. Lu, T. Xiang, X. L. Huang, C. Li, W. F. Zhao and Q. Zhang, *Carbohydr. Polym.*, 2015, **133**, 587–595.

58 F. C. Wu, R. L. Tsengand and R. S. Juang, *Chem. Eng. J.*, 2009, **153**, 1–8.

59 Y. Huang, Y. Miao and T. Liu, *J. Appl. Polym. Sci.*, 2014, **131**, 5829–5836.

60 M. J. Park, G. M. Nisola, A. B. Beltran, R. E. C. Torrejos, J. G. Seo and S. P. Lee, *Chem. Eng. J.*, 2014, **254**, 73–81.